RSC Advances

This article can be cited before page numbers have been issued, to do this please use: Z. Gao, F. Liu, J. Li, G. Cheng and P. Lu, *RSC Adv.*, 2016, DOI: 10.1039/C6RA18755B.

ROYAL SOCIETY OF CHEMISTRY

www.rsc.org/advances

View Article Online
DOI: 10.1039/C6RA18755B

Journal Name

ARTICLE

Solution-processed UV Light Emitting Diode Based on Butyltriphenylsilane Modified Phenanthro[9, 10-*d*]imidazole with High Efficiency

Received 00th January 20xx,
Accepted 00th January 20xx

DOI: 10.1039/x0xx00000x

www.rsc.org/

Zhao Gao,[a,c] Fangming Liu,[a] Jinyu Li,[a] Gang Cheng,[b,*] and Ping Lu[a,*]

A new UV fluorescent material based on phenanthro[9, 10-*d*]imidazole and butyltriphenylsilane (SiBPI) is designed and synthesized, which presents high quantum yield and excellent solubility. A non-doped solution-processed device using SiBPI as active layer achieves an extremely high η_{ext} of 1.76% with guaranteed saturated UV CIE coordinates of (0.158, 0.042).

1. Introduction

Solution-processable small organic light emitting materials, which possess concise structure and good solubility, have attracted much attentions in both scientific and industrial communities as potential candidates for large-scale flat-panel displays and low-cost solid-state lightings.[1-3] Remarkable progress has been made in achieving high-quality solution-processable materials that emit colors in the visible region over the past decade.[4-7] Materials with even shorter ultraviolet (UV) wavelengths, however, are not developed as well, although efficient UV emitters are of great importance in biology medical treatment,[8] sterilization,[9] and high density information storage.[10] In addition, such emitters can also be used to generate light of all colors by energy transfer to emissive dopants,[11-12] and can effectively reduce the power consumption of a full-color organic light emitting diodes (OLEDs).[13-16] According to the European Broadcasting Union (EBU) standard blue Commission International de L'Eclairage (CIE) coordinates of (0.15, 0.06),[17] UV OLEDs should match the emission with y CIE coordinate lower than 0.06.

In our prior study, phenanthro[9, 10-*d*]imidazole (PI) was found to be a promising building block for UV emitting materials which possesses a wide energy bandgap of 3.46 eV, violet light emission in film (393 nm), and narrow full width half maximum (FWHM, 50 nm).[6,18] Moreover, PI also exhibits ambipolar carrier transport properties with high carrier mobilities, which is quite beneficial for its application for OLEDs.[19-20] However, its low glass transition temperature (T_g) of 62 °C, moderate solid-state quantum yield of 40% and poor film-forming ability is far from being adequate for application in UV light emitting OLEDs. In addition, most of excellent PI-based emitters exhibit nearly unity fluorescence quantum efficiency and UV emission in dilute solution. Unfortunately, they tend to aggregation in the solid state, which usually results in the decreased efficiency and emission out of the UV spectral region in OLEDs.[18,21-22] This problem can be solved to some extent by introducing a bulky silane segment, which enhances the solid state efficiency by the tetrahedral geometry as well as maintains the wide bandgap of PI.[6] In this paper, the tetrahedral geometry of silane segment could increase the steric hindrance, suppress intermolecular interactions and enhance the efficiency in solid state. Compared with PPI (0.40), very high PL quantum yield of 0.77 for SiBPI is observed in thin films. What is more, the bandgap of PPI and SiBPI are all calculated to be 3.28 eV according to their absorption edge in film state. It indicates that the bulky silane moiety effectively blocked the quenching process of PPI in film. Contrast with PPI, the T_g and T_m of SiBPI are also improved. In this paper, we further increase the solubility of PI-based materials by adopting butyltriphenylsilane as a substituent, which could effectively increase the flexibility of the compound to help conserve better morphological stability with convenient solution-processibility. As a result, SiBPI shows high solubility as high as 80 mg mL^{-1} in toluene. The solution-processed device based on SiBPI exhibits good performance with the maximum external quantum efficiency (η_{ext}) of 1.76%, current efficiency (η_c) of 0.57 cd A^{-1}, and CIE coordinates of (0.158, 0.042), which is comparable to the performance of its vacuum-deposited device. To the best of our knowledge, this newly synthesized material shows the guaranteed saturated UV electroluminescence (EL) with high efficiency by spin-coating method.

[a] State Key Laboratory of Supramolecular Structure and Materials, Jilin University, 2699 Qianjin Avenue, Changchun, 130012, China. E-mail: lup@jlu.edu.cn
[b] State Key Laboratory on Integrated Optoelectronics, College of Electronic Science and Engineering, Jilin University, 2699 Qianjin Avenue, Changchun 130012, China. E-mail: chenggang@jlu.edu.cn
[c] National Key Laboratory for Shock Wave and Detonation Physics Research, Institute of Fluid Physics, Chinese Academy of Engineering Physics, Mianyang 621900, China.

† Electronic Supplementary Information (ESI) available. See DOI: 10.1039/x0xx00000x

View Article Online
DOI: 10.1039/C6RA18755B

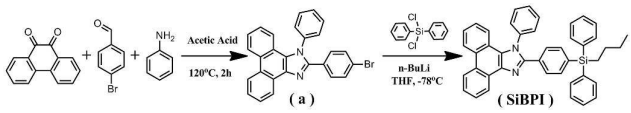

Scheme 1. The synthetic route of SiBPI.

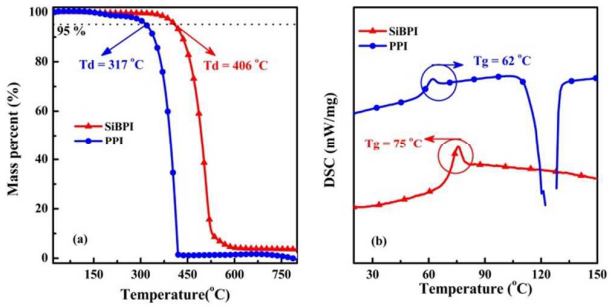

Fig. 1 The TGA and DSC graphs of SiBPI and PPI (recorded at a heating rate of 10 K min^{-1} under a nitrogen flow).

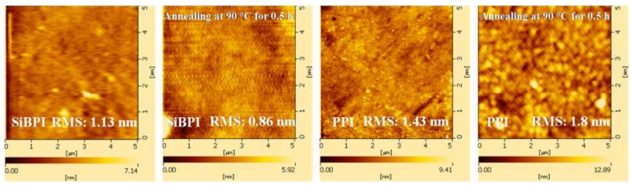

Fig. 2 The spin-coating films of SiBPI and PPI on the quartz plate at room temperature and after annealing at 90 °C for 0.5 h.

2. Results and discussion

2.1 Synthesis

The synthesis route to SiBPI is shown in Scheme 1. Firstly, the reaction intermediate (**a**) was readily obtained by "one-pot" Debus-Radziszewski reaction with high yield according to our reported procedure.[21] Then, SiBPI used for this study could be achieved by treating a with n-BuLi at -78 °C, followed by lithium exchange with dichlorodiphenylsilane.[23] The molecular structure of the intermediate and final product were confirmed by ^{1}H NMR, high-resolution mass spectrometry, fourier-transform infrared spectroscopy, elemental analysis, and corresponded well with their expected structure (Supporting Information).

2.2 Thermal properties

SiBPI exhibited decomposition temperature (T_d, corresponding to 5% weight loss) of 406 °C by thermmogravimetric analysis (TGA), which was much higher than PPI (317 °C) (Fig. 1) due to the introduction of butyltriphenylsilane segment. The T_g of SiBPI was measured to be at 75 °C by differential scanning calorimetric (DSC). Upon further heating beyond T_g, no exothermal peak of crystallization temperature was observed. Atomic force microscopy (AFM) characterization presented that film of SiBPI fabricated by spin-coating method displayed fairly homogenous and smooth surface morphology with the roughness of 1.13 nm. After annealing at 90 °C for 0.5 h, the film morphology were almost kept unchanged. In contrast, the surface of PPI film showed noticeable crystallization area especially after annealing (Fig. 2). The thermal stability and film morphology of SiBPI had been successfully modified for application in UV devices with the rational design of molecular structure. As a consequence, SiBPI might form morphologically stable films during device operation, which is highly important for its application.[24-25]

2.3 Photophysical properties

SiBPI emitted in UV region showing quite similar emission spectra as PPI in dilute THF solution (Fig. 3), indicating that the non-conjugated silane segment in SiBPI did not affect the conjugation length and the bandgap in comparison with PPI. The emission peaks of PPI and SiBPI were both located at 369 nm and 372 nm, respectively. It is noteworthy that SiBPI exhibited narrow emission with only 36 nm FWHM in the spectra. This is helpful for obtaining saturated color with a low y CIE coordinate in OLEDs. We also measured the fluorescence in different solvents with various polarities, and SiBPI showed almost the similar emission spectra, implying that no obvious intramolecular charge transfer existed in the compound (Fig. 4). SiBPI and PPI also exhibited similar absorption spectra. The maximum absorption peak at 262 nm was attributed to the isolated benzene ring connected with imidazole. The absorption band around 340 nm of SiBPI was a little bit red-shifted compared with that of PPI, which might be originated from the π-π* transition of PI unit. The bandgap of PPI and SiBPI were all calculated to be 3.28 eV according to their absorption edge in film state. Very high PL quantum yield of 0.77 for SiBPI was observed in thin films indicating that the bulky silane moiety effectively blocked the quenching process of PPI in film. Such high quantum efficiency was unusually observed for wide bandgap organic UV emitters.[26] What is more, the introduction of silane segment and butyl unit could effectively afford the materials with convenient solution-

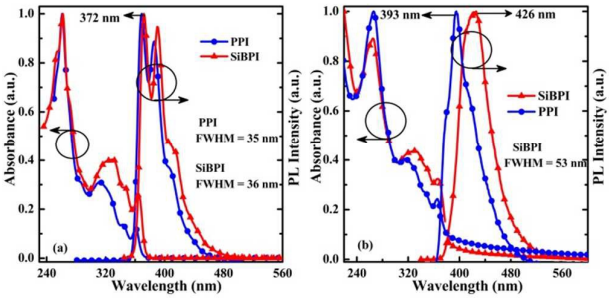

Fig. 3 (a) Normalized absorption and emission spectra of SiBPI in THF (concentration: 10^{-5} mol L^{-1}) and (b) Normalized absorption and emission spectra in film, compared with PPI.

View Article Online
DOI: 10.1039/C6RA18755B

Journal Name

ARTICLE

Table 1 The photophysical, thermal and electrochemistry data of PPI and SiBPI.

	$\lambda^{PL}_{max\ soln}$ [a)] [nm]	$FWHM_{soln}$ [b)] [nm]	$\lambda^{PL}_{max\ film}$ [c)] [nm]	$FWHM_{film}$ [d)] [nm]	Φ_{fl} [e)] [%]	T_g [°C]	T_m [°C]	T_d [°C]	HOMO [f)] [eV]	LUMO [f)] [eV]	ΔE_g [f)] [eV]
PPI	369	35	393	50	40	62	126	317	-5.53	-2.07	3.46
SiBPI	372	36	426	53	77	75	190	406	-5.57	-2.22	3.35

[a)] The maximum emission peaks in THF (concentration: 10^{-5} mol L^{-1}); [b)] The full width half maximum of emission in THF (concentration: 10^{-5} mol L^{-1}); [c)] The maximum emission peaks in film; [d)] The full width half maximum of emission in film; [e)] The PL quantum yield in thin film; [f)] Measured by cyclic voltammetry.

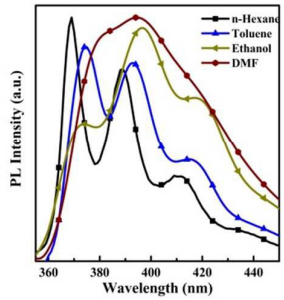

Fig. 4 PL spectra of SiBPI, measured in different solvents with easing polarity (concentration: 10^{-5} mol L^{-1}).

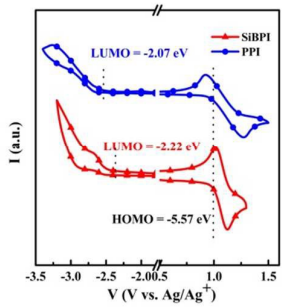

Fig. 5 Cyclic voltammogram of the SiBPI and PPI.

processibility. The solubility as high as 80 mg mL^{-1} in toluene was attained for SiBPI, suggesting the greatly improved flexibility as compared to PPI. Such an exceedingly high solubility could guarantee SiBPI as potential candidate for solution-processable material to be applied in large-scale flat-panel displays and low-cost solid-state lightings.

2.4 Electrochemical properties and theoretical calculation

The highest occupied molecular orbital (HOMO) and lowest unoccupied (LUMO) levels were measured by cyclic voltammetry using a glassy carbon disk (diameter 3 mm) as the working electrode, a platinum wire as the auxiliary electrode with a porous ceramic wick, and Ag/Ag^+ as the reference electrode (Fig. 5).[27-28] PPI exhibited one quasi-reversible oxidation wave with an oxidation onset potential of 0.95 V, which gave a HOMO level of -5.53 eV by comparison to ferrocene (E_{HOMO} = - (eE_{ox}+4.58) eV), and the LUMO level was measured to be -2.07 eV. SiBPI also exhibited one quasi-reversible oxidation wave corresponding to HOMO level of -5.57 eV. While the LUMO level was calculated to be -2.22 eV for SiBPI (much lower than that of PPI), which may be attributed to the partly overlapping between π-π* conjugation in PPI and the d orbital of Si atom. The decreased LUMO level was beneficial effect for the electron injection in device. This effect was often observed in silicon-containing compounds.[23] The molecular design concept is further validated by the

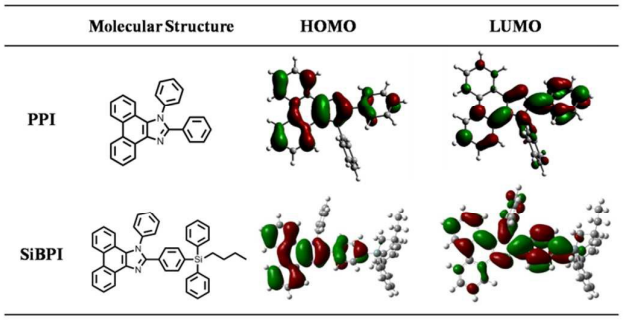

Fig. 6 Frontier molecular orbitals (HOMO and LUMO) of PPI and SiBPI calculated with DFT on B3LYP/6-31G(d) level.

View Article Online
DOI: 10.1039/C6RA18755B

Journal Name

ARTICLE

Table 2 Performance of the vacuum-deposited device A and the solution-processed device B.

Device[a)]	λ_{max}, EL [nm]	V_{on} [V]	η_{ext}[b)] [%, 100 cd m^{-2}]	$\eta_{max, ext}$[c)] [%]	L_{max}[d)] [cd m^{-2}]	η_c[e)] [cd A^{-1}]	CIE[f)] [x, y]	CIE[g)] [x, y, 100 cd m^{-2}]
A	424	3.8	2.05	2.62	693	1.04	(0.166, 0.046)	(0.194, 0.078)
B	416	5.3	1.70	1.76	420	0.57	(0.158, 0.042)	(0.159, 0.044)

[a)] The structure of device A: ITO/MoO_3 (10 nm)/TAPC (40 nm)/ SiBPI (20 nm) /TmPyPb (40 nm)/LiF (0.5 nm)/Al (100 nm); device B: ITO/PEDOT:PSS/ SiBPI (10 mg/mL)/TmPyPb (5 nm)/TPBi (40 nm)/LiF (1.2 nm)/Al (150 nm); [b)] The external of quantum efficiency (η_{ext}) taken at 100 cd m^{-2}; [c)] The maximum external of quantum efficiency ($\eta_{max, ext}$); [d)] The maximum values of luminance (L_{max}); [e)] The current efficiency (η_c); [f)] The CIE coordinates taken at 6 V; [g)] The CIE coordinates taken at 100 cd m^{-2}.

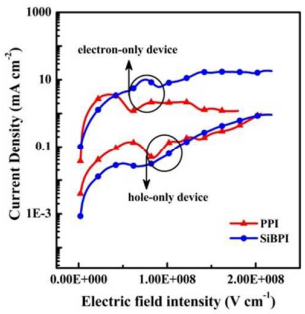

Fig. 7 The current density-electric field intensity curves of the single carrier devices based on PPI and SiBPI.

theoretical calculation. As shown in Fig. 6, the density function theory (DFT) calculated HOMO and LUMO were found to be mainly localized on the PI moiety. The observations are in a good agreement with the experimental results.

2.5 Electroluminescent properties

To investigate the carrier injection and transport ability, the hole-only and the electron-only devices of SiBPI and PPI were fabricated. The configuration of the hole-only device was ITO/PEDOT/SiBPI or PPI (80 nm)/Au and the electron-only device had the configuration of ITO/TPBi (10 nm)/ SiBPI or PPI (100 nm)/LiF/Al. In the hole-only device, the results indicated that the hole current values of SiBPI and PPI were not much different. In the electron-only device, the 10 nm TPBi was inserted as a hole-blocking layer to ensure a pure electron current in the device. The electric field intensity was calculated by the voltage and the thickness of the film obtained in the deposition process. As shown in Fig. 7, in the high electric field intensity zone (> 4.2*10^7 V cm^{-1}), the electron current values of SiBPI was approximately one order magnitude higher than that of PPI, providing strong evidence that SiBPI could possess better electron injection and transport ability.

To further access the performance of SiBPI as a UV light-emitter, non-doped vacuum-deposited device (A) and spin-coating device (B) were both fabricated. Device A was a typical sandwiched structure of ITO/MoO_3 (10 nm)/TAPC (40 nm)/ SiBPI (20 nm)/TmPyPb (40 nm)/LiF (0.5 nm)/Al (100 nm). The best EL performance in terms of η_{ext} (2.62%) was obtained, with η_c of 1.04 cd A^{-1} (Table 2). And it showed a relatively low turn-on voltage of 3.8 V, which was different from the other OLEDs containing wide bandgap emitters. The device exhibited UV EL spectrum similar with its thin film PL spectrum. The maximum peak of EL emission was at 424 nm for SiBPI with very narrow spectra distribution (FWHM = 60 nm), which was very helpful for obtaining saturated UV color. The CIE coordinates of (0.166, 0.046) matched well with the requirement of EBU standard blue CIE coordinate.[29-30] As shown in Fig. S5, the emission at 424 nm for vacuum deposition device A can be ascribed to be the emission from SiBPI. However, at high voltages, distinct long-wavelength emission around 584 nm was observed for vacuum deposition device A, which might be generated by an exciplex formed at the interface.[31-32]

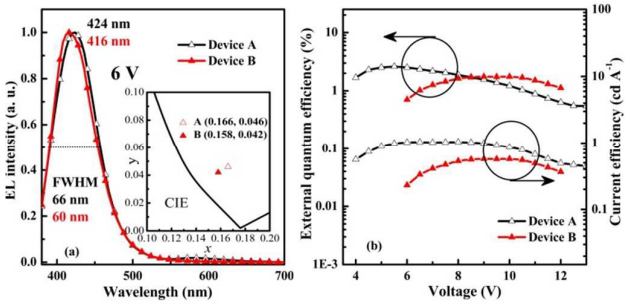

Fig. 8 (a) EL emission for devices A and B at 6 V. Insert: the CIE coordinates. (b) The external quantum efficiency and current efficiency for devices A and B.

View Article Online
DOI: 10.1039/C6RA18755B

Journal Name

ARTICLE

Table 3 Data summary of deep blue devices with high efficiency by solution-processed.

emitters	$\eta_{c,\,max}$ [a] (cd A^{-1})	$\eta_{p,\,max}$ [b] (lm W^{-1})	$\eta_{ext,\,max}$ [c] (%)	L_{max} [d] (cd m^{-2})	$\lambda_{max,\,EL}$ [e] (nm)	CIE [f] (x,y)	Ref
p-DTPABI-Cz	3.71	2.32	2.88	5521	461	0.16, 0.17	33
m-DTPABI-Cz	2.74	1.73	2.28	4403	465	0.16, 0.16	33
OCSoC	4.0	3.0	-	5500	455	0.172, 0.224	34
1a	3.79	-	-	19181	415	0.17, 0.11	35
3a	0.5	0.2	1.50	714	415	0.16,0.05	36
5P-TCTA	2.48	2.15	2.30	7300	445	0.15,0.09	37
TFPC2	0.86	0.56	2.02	1054	430	0.16,0.04	38
POSS-DPCz	1.4	-	0.92	8900	450	0.15,0.12	39
5CzCN	-	-	18.7	-	-	0.17,0.27	40
HFB-diF-Dpa	6.99	6.10	5.45	5000	460	0.154,0.136	41
TPA-PyF3	1.13	0.66	1.78	1352	423	0.16,0.07	42
CBP-PyF3	1.68	1.08	2.07	1289	423	0.16,0.08	42
2	0.47	0.18	1.25	483.1	431	0.157,0.069	43

[a] The maximum current efficiency ($\eta_{c,\,max}$); [b] The maximum power efficiency ($\eta_{p,\,max}$); [c] The maximum external of quantum efficiency ($\eta_{ext,\,max}$); [d] The maximum values of luminance (L_{max}); [e] The maximum peak of electroluminescence emission ($\lambda_{max,\,EL}$); [f] The CIE coordinates taken at turn-on voltage.

Accordingly, we could assume that the recombination zone for the typical sandwiched structure was located near the HTL/ETL interface. So, at 100 cd m^{-2} the CIE coordinates were changed to (0.194, 0.078).

Devices B was fabricated by spin-coating method with the structure of ITO/PEDOT:PSS/ SiBPI (60 nm)/TmPyPb (5 nm)/TPBi (40 nm)/LiF (1.2 nm)/Al (150 nm). It exhibited high performance with the maximum η_{ext} of 1.76 %, η_c of 0.57 cd A^{-1}, and CIE coordinates of (0.158, 0.042). Significantly, at 100 cd m^{-2} the CIE coordinates were still kept at (0.159, 0.044), indicating very good color stability for UV light-emitting diodes over a wide range of operation conditions. The EL emission spectrum was as similar as that obtained from the PL emission spectrum. In particular, the EL spectra and CIE coordinates were kept unchanged over the entire applied voltage from 6 V to 11 V. The data of newly published deep blue devices by spin-coating method were list as comparison. This is the highest spin-coating UV EL efficiency in comparison with previously reported result, which is consistent with its high thin film photo luminescent quantum yield, appropriate flexibility and high T_g, and indicated the present device structure could effectively confine the carriers and excitons in the emissive layer. Moreover, it is worthy to note that SiBPI showed very low roll-off of the luminance efficiencies. The results further demonstrated that the molecular design strategy is feasible.

Conclusions

In summary, a new highly efficient UV emitter based on PPI has been designed, synthesized and fully characterized. The promising photophysical properties of SiBPI, including high

View Article Online
DOI: 10.1039/C6RA18755B

quantum yield of UV emission, appropriate flexibility, high thermal and morphological stability can be distinctly ascribed to the introduction of butyltriphenylsilane. In addition, the solubility as high as 80 mg mL^{-1} in toluene was attained for SiBPI. The solution-processed device based on SiBPI can achieve an excellent η_{ext} of 1.76% with true violet CIE coordinates of (0.158, 0.042), which is comparable to the performance of its vacuum-deposited device. Over a wide range of operation conditions, the luminance efficiencies and color purity were almost unchanged. It was among the best results ever reported for solution-processed UV light-emitting diodes, which inspired its application in the future.

Experimental

Synthesis of 2-(4-bromophenyl)-1-phenyl-3a,11b-dihydro-1H-phenanthro[9,10-d]imidazole (a)

A mixture of 4-bromobenzaldehyde (2.5 g, 13.5 mmol), phenanthrene-9,10-dione (2.8 g, 13.5 mmol), aniline (6.3 mL, 67.5 mmol), ammonium acetate (4.2 g, 54.5 mmol), and acetic acid (60 mL) were refluxed under nitrogen in an oil bath. After 2 h, the mixture was cooled and filtered. The solid product was washed with acetic acid many times. Then it is obtained the product as white powder (5.5 g). Yield: 90.6 %. ^{1}H NMR (500 MHz, DMSO, δ): 8.95 (d, *J* = 8.36 Hz, 1 H), 8.90 (d, *J* = 8.38 Hz, 1 H), 8.70 (d, *J* = 7.95 Hz, 1H), 7.80 (t, *J* = 7.16 Hz, 7.72 Hz, 1H), 7.76-7.69 (m, 6H), 7.59 (t, *J* = 8.56 Hz, 8.72 Hz, 3 H), 7.53 (d, *J* = 8.61 Hz, 2H), 7.37 (t, *J* = 7.36 Hz, 7.97 Hz, 1H), 7.10 (d, *J* = 8.34 Hz, 1H); MALDI-TOF (*m/z*): [M^+] calcd for $C_{27}H_{17}BrN_2$: 449.3; Found: 449.0.

Synthesis of 2-(4-(butyldiphenylsilyl)phenyl)-1-phenyl-1H-phenanthro[9,10-d]imidazole (SiBPI)

A solution of *n*-BuLi in hexane (2.4 M, 6.0 mL) was added slowly (over 1 h) under nitrogen to a stirred solution of **a** (5 g, 11.1 mmol) in anhydrous THF (150 mL) at -78 ^{o}C. Dichlorodiphenylsilane (1.4 g, 5.6 mmol) was then added quickly while maintaining the temperature at -78 ^{o}C. The color of the solution gradually changed to pale yellow. After 4 h the mixture was warmed to room temperature and stirred for 24 h. The reaction mixture was then quenched with water and extracted with chloroform. The combined organic phases were dried ($MgSO_4$) and concentrated under reduced pressure. After solvent evaporation, the liquid was purified by column chromatography using petroleum ether/ methylene chloride as the eluent to afford a white solid (2.0 g). Yield: 59 %; ^{1}H NMR (500 MHz, DMSO, δ): 8.94 (d, *J* = 8.31 Hz, 1 H), 8.88 (d, *J* = 8.55 Hz, 1 H), 8.69 (d, *J* = 7.97 Hz, 1H), 7.79 (t, *J* = 7.12 Hz, 7.90 Hz, 1H), 7.73-7.67 (m, 6H), 7.63 (d, *J* = 8.22 Hz, 2 H), 7.57 (t, *J* = 7.12 Hz, 8.29 Hz, 1H),7.46-7.39 (m, 12H), 7.35 (t, *J* = 7.48 Hz, 8.1 Hz, 1H), 7.06 (d, *J* = 8.28 Hz, 1H), 1.34 (d, *J* = 8.43 Hz, 6H), 0.94 (t, *J* = 6.64 Hz, 6.92 Hz, 3H); FTIR (KBr, ν, cm^{-1}): 3048, 2946, 2918, 2860, 1593, 1513, 1491, 1466, 1451, 1425, 1394, 1373, 1296, 1196, 1107, 1016, 999, 962, 873, 826, 806, 755, 723, 699, 615, 552, 532, 509, 486, 469, 428; MALDI-TOF (*m/z*): [M^+] calcd for $C_{43}H_{36}N_2Si$: 608.8; Found: 608.8. Anal. calcd for $C_{43}H_{36}N_2Si$: C 84.83, H 5.96, N 4.60; Found: C 84.99, H 5.99, N 4.53.

Acknowledgements

This work was supported financially by the Ministry of Science and Technology of China (2013CB834801), the National Science Foundation of China (21374038) and the Jilin Provincial Science and Technology Department (20160101302JC).

References

1 A. C. Arias, J. D. MacKenzie, I. McCulloch, J. Rivnay , A. Salleo, *Chem. Rev.*, 2010, **110**, 3.
2 S. Ameen, J. Lee, H. Han, M. C. Suh, C. Lee, *RSC Adv.*, 2016, **6**, 33212.
3 Z. Wang, Y. Lou, S. Naka and H. Okada, *ACS Appl. Mater. Interfaces*, 2011, **3**, 2496.
4 R. Zhao, W. Zhang, Y. Ma, *Acta Polym. Sin.*, 2011, **9**, 985.
5 S. Gong, Q. Fu, Q. Wang, C. Yang, C. Zhong, J. Qin and D. Ma, *Adv. Mater.*, 2011, **23**, 4956.
6 Z. Gao, G. Cheng, F. Shen, S. Zhang, Y. Zhang, P. Lu and Y. Ma, *Laser & Photonics Rev.*, 2014, **8**, L6.
7 Y. Tian, X. Xu and L. Li, *RSC Adv.*, 2015, **5**, 98075.
8 S. Landgraf, *J. Biochem. Biophys. Methods*, 2004, **61**, 125.
9 L. T. T. Nhung, H. Nagata, A. Takahashi, M. Aihara, T. Okamoto, T. Shimohata, K. Mawatari, M. Akutagawa, Y. Kinouchi, M. Haraguchi, *J. Med. Investig.*, 2012, **59**, 53.
10 H. van Santen, J. H. M. Neijzen, *Jpn. J. Appl. Phys. Part 1*, 2003, 42, 1110.
11 K. Wang, F. C. Zhao, C. G. Wang, S. Y. Chen, D. Chen, H. Y. Zhang, Y. Liu, D. G. Ma, Y. Wang, *Adv. Funct. Mater.*, 2013, **23**, 2672.
12 H. Huang, Y. X. Wang, S. Q. Zhuang, X. Yang, L. Wang, C. L. Yang, *J. Phys. Chem. C.,* 2012, **116**, 19458.
13 M. T. Lee, H. H. Chen, C. H. Liao, C. H. Tsai, C. H. Chen, *Appl. Phys. Lett.*, 2004, **85**, 3301.
14 M. T. Lee, C. H. Liao, C. H. Tsai, C. H. Chen, *Adv. Mater.*, 2005, **17**, 2493.
15 A. Kraft, A. C. Grimsdale, A. B. Holmes, *Angew. Chem. Int. Ed.*, 1998, **37**, 402.
16 Y. J. Tung, T. Nago, M. Hack, J. Brown, N. Koide, Y. Nagara, Y. Kato, H. Ito, *SID 2004 Technical Digest.*, 2004, **35**, 48.
17 N. T. Gurin, K. V. Paksyutov, M. A. Terent'ev, A. V. Shirokov, *Tech. Phys.*, 2012, **57**, 308.
18 Z. M. Wang, P. Lu, S. M. Chen, Z. Gao, F. Z. Shen, W. S. Zhang, Y. X. Xu, H. S. Kwok, Y. G. Ma, *J. Mater. Chem.,* 2011, **21**, 5451.
19 W. C. Chen, Y. Yuan, G. F. Wu, H. X. Wei, L. Tang, Q. X. Tong, F. L. Wong and C. S. Lee, *Adv. Opt. Mater.*, 2014, **2**, 626.
20 Y. Yuan, D. Li, X. Zhang, X. Zhao, Y. Liu, J. Zhang and Y. Wang, *New J. Chem.*, 2011, **35**, 1534.
21 Z. Gao, Z. Wang, T. Shan, Y. Liu, F. Shen, Y. Pan, H. Zhang, X. He, P. Lu, B. Yang and Y. Ma, *Org. Electron.*, 2014, **15**, 2667.
22 Z. Gao, Y. Liu, Z. Wang, F. Shen, H. Liu, G. Sun, L. Yao, Y. Lv, P. Lu and Y. Ma, *Chem. Eur. J.*, 2013, **19**, 2602.
23 D. H. Hu, F. Z. Shen, H. Liu, P. Lu, Y. Lv, D. D. Liu, and Y. G. Ma, *Chem. Commun.*, 2012, **48**, 3015.
24 S. Tokito, H. Tanaka, K. Noda, A. Okada, Y. Taga, *Appl. Phys. Lett.*, 1997, **70**, 1929.
25 Z. K. Chen, H. Meng, Y. H. Lai, W. Huang, *Macromolecules*, 1999, **32**, 4351.
26 S. H. Kim, I. Cho, M. K. Sim, S. Park, S. Y. Park, *J. Mater. Chem.*, 2011, **21**, 9139.

View Article Online
DOI: 10.1039/C6RA18755B

27 G. Gritzner and J. Kuta, *Pure Appl. Chem.*, 1984, **56**, 461.
28 J. H. Kim and H. Lee, *Synth. Met.*, 2004, **144**, 169.
29 M. Zhu, C. Yang, *Chem. Soc. Rev.*, 2013, **42**, 4963.
30 R. Kim, S. Lee, K. H. Kim, Y. J. Lee, S. K. Kwon, J. J. Kim, Y. H. Kim, *Chem. Commun.*, 2013, **49**, 4664.
31 M. Zhu, T. Ye, C. Li, X. Cao, C. Zhong, D. Ma, J. Qin, C. Yang, *J. Phys. Chem. C*, 2011, **115**, 17965.
32 G. Hughes, M. R. Bryce, *J. Mater. Chem.*, 2005, **15**, 94.
33 Y. Bai, L. Hong, T. Lei, L. Zhang, X. Ouyang, Z. Liu, Y. Chen, W. Li, Z. Ge, *Dyes Pigm.*, 2016, **132**, 94.
34 S. Xue, X. Qiu, L. Yao, L. Wang, M. Yao, C. Gu, Y. Wang, Z. Xie, H. Wu, *Org. Electron.*, 2015, **27**, 35.
35 T. Sudyoadsuk, P. Moonsin, N. Prachumrak, S. Namuangruk, S. Jungsuttiwong, T. Keawina, V. Promarak, *Polym. Chem.*, 2014, **5**, 3982.
36 D. Karthik, K. R. J. Thomas, J. Jou, S. Kumar, Y. Chen, Y. Jou, *RSC Adv.*, 2015, **5**, 8727.
37 M. Yu, S. Wang, S. Shao, J. Ding, L. Wang, X. Jing, F. Wang, *J. Mater. Chem. C*, 2015, **3**, 861.
38 L. Zhao, S. Wang, S. Shao, J. Ding, L. Wang, X. Jing, F. Wang, *J. Mater. Chem. C*, 2015, **3**, 8895.
39 C. Cheng, Y. Chu, C. Chu, D. Lee, *J. Mater. Chem. C*, 2016, **4**, 6461.
40 Y. J. Cho, S. K. Jeon, J. Y. Lee, *Adv. Optical Mater.*, 2016, **4**, 688.
41 C. Liu, Q. Fu, Y. Zou, C. Yang, D. Ma, J. Qin, *Chem. Mater.*, 2014, **26**, 3074.
42 Z. Fan, N. Li, Y. Quan, Q. Chen, S. Ye, Q. Fan, and W. Huang, *J. Polym. Sci. Pol. Chem.*, 2016, **54**, 795.
43 A. L. Fisher, K. E. Linton, K. T. Kamtekar, C. Pearson, M. R. Bryce, M. C. Petty, *Chem. Mater.*, 2011, **23**, 1640.

View Article Online
DOI: 10.1039/C6RA18755B

Table of contents

A solution-processed device using SiBPI as active layer achieves an high η_{ext} of 1.76% with CIE coordinates of (0.158, 0.042).